

# SIL/HIL Replication of Electric Aircraft Powertrain Dynamics and Inner-Loop Control for V&V of System Health Management Routines

Brian Bole<sup>1</sup>, Christopher Teubert<sup>2</sup>, Quach Cuong Chi<sup>3</sup>, Hogge Edward<sup>3</sup>, Sixto Vazquez<sup>3</sup>, Kai Goebel<sup>4</sup>, Vachtsevanos George<sup>1</sup>

<sup>1</sup> *Department of Electrical and Computer Engineering, Georgia Institute of Technology, Atlanta, GA, 30332, USA*  
*bbole3@gatech.edu*

<sup>2</sup> *SGT, Inc., NASA Ames Research Center, Moffett Field, CA, 94035, USA*  
*Christopher.A.Teubert@nasa.gov*

<sup>3</sup> *NASA Langley Research Center, Hampton, VA 23681, USA*  
*cquach@nasa.gov*

<sup>4</sup> *NASA Ames Research Center, Moffett Field, CA 94035, USA*  
*kai.goebel@nasa.gov*

## ABSTRACT

Software-in-the-loop and Hardware-in-the-loop testing of failure prognostics and decision making tools for aircraft systems will facilitate more comprehensive and cost-effective testing than what is practical to conduct with flight tests. A framework is described for the offline recreation of dynamic loads on simulated or physical aircraft powertrain components based on a real-time simulation of airframe dynamics running on a flight simulator, an inner-loop flight control policy executed by either an autopilot routine or a human pilot, and a supervisory fault management control policy. The creation of an offline framework for verifying and validating supervisory failure prognostics and decision making routines is described for the example of battery charge depletion failure scenarios onboard a prototype electric unmanned aerial vehicle.

## 1. INTRODUCTION

An early investment of resources into the development of an offline verification and validation (V&V) testing infrastructure for prognostics and supervisory health management algorithms is easily justified for complex systems in which online testing is substantially more time consuming and costly than offline testing. The V&V process is used to confirm that algorithms meet requirements, and perform in a way that is

consistent with stakeholder expectations. Flight tests prior to algorithm V&V can be dangerous to the vehicle, pilot, and ground crew. Offline tests to V&V algorithms in a laboratory setting prior to flight tests will not only improve flight test safety, but, as many issues can be resolved during offline tests, it reduces the number of real flight tests required for V&V, therefore reducing cost and development time.

Offline V&V tests of supervisory failure prognosis and decision making routines will allow developed supervisory algorithms to interact with onboard flight controllers and measured flight data exactly as they would during flight tests. The offline testing of health management algorithms may be conducted using Software-in-the-loop (SIL) or Hardware-in-the-loop (HIL) procedures. SIL testing refers to tests conducted using only software simulations of system physics and embedded control routines. HIL testing refers to tests that include some hardware components from the target system.

When conducting V&V of supervisory control algorithms, injecting faults and testing to failure can provide valuable knowledge of the algorithm's behavior during potential failure scenarios. It is often not feasible to test to failure during flight tests without compromising the safety of the vehicle, onboard crew (for manned aircraft), or the ground crew. It is therefore valuable to have a method for the offline V&V of algorithm performance during failure scenarios. Supervisory control algorithms can also be tested over a wide range of potential environmental conditions in offline V&V, including extreme conditions that are rarely encountered in practice. That said however, offline V&V testing is limited by the accu-

Brian Bole et al. This is an open-access article distributed under the terms of the Creative Commons Attribution 3.0 United States License, which permits unrestricted use, distribution, and reproduction in any medium, provided the original author and source are credited.

racy of SIL and HIL replications of nominal and off-nominal system dynamics, and flight testing is still a necessary part of the algorithm development and V&V process.

The SIL/HIL testing framework described in this paper uses the X-Plane flight simulator package and an X-Plane Toolbox for MATLAB to facilitate prognostic based control algorithm V&V over a range of potential operating conditions. Examples of other offline testbeds making use of X-Plane for aerodynamics simulation and Matlab/Simulink softwares for simulation of control routines is found in (ibeiro & Oliveira, 2010; Brown & Garcia, 2009; Sagoo et al., 2010). The SIL/HIL testbed presented in this paper improves present capabilities for performing offline testing with X-Plane aerodynamics simulations, by including a structure for simulating internal aircraft dynamics and component fault scenarios in MATLAB simulations and in HIL realizations. The communications architecture developed to interface supervisory control routines running in MATLAB to SIL/HIL tests and aerodynamics simulation running in X-Plane is intended to be distributed open-source in the near future.

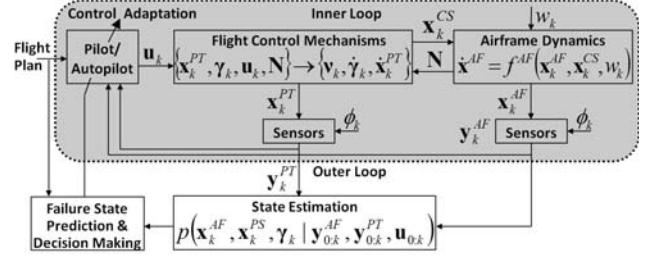
The general framework for SIL/HIL testing is described in Section 2. The development of an SIL/HIL simulation structure for the offline testing of battery charge management algorithms onboard an Edge-540 flight vehicle is presented in Section 3.

## 2. GENERAL FRAMEWORK

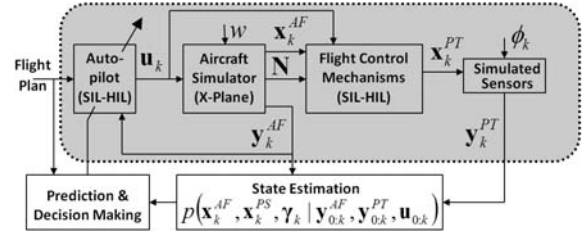
This section introduces an SIL/HIL framework for testing component failure prognostics and real-time supervisory decision making algorithms that are intended to run onboard a flight vehicle. Block diagrams illustrating the structure of control loops used for online and offline flight testing are shown in Figure 1. The symbols used in Figure 1 and elsewhere in the paper are defined in the Nomenclature table at the end of the paper. For both online and offline control testing it is assumed that an inner-loop controller updates flight control inputs based on a known flight plan and observations of the system state. Failure prognostics and supervisory decision making operations are performed by an outer-loop controller. Inner control loops for both online and offline testing cases are described in the following subsection

### 2.1. Inner-Loop Control Dynamics

In both online and offline vehicle controls testing cases, a human pilot or a pre-programmed autopilot, provides closed-loop control by updating the control vector,  $\mathbf{u}$ . Both human pilot and autopilot will henceforth be referred to as just 'the pilot', for convenience. Measurements of the position, speed, and orientation of a flight vehicle and its control surfaces, represented by the airframe observation vector  $\mathbf{y}^{AF}$ , are used by the pilot along with a vehicle flight plan.



(a) Inner and outer control loops for online testing



(b) Inner and outer control loops for offline testing

Figure 1. Closed-loop control for online and offline flight testing

The 'Flight Control Mechanisms' block shown in Figure 1(a) represents the internal electrical and mechanical dynamics of the vehicle's powertrain. The inner-loop control signals sent by the pilot, and the aerodynamic forces exerted on the vehicle's control surfaces by the surrounding environment,  $\mathbf{N}$ , are inputs to this block. The  $\mathbf{N}$  vector consists of forces like the drag on a propeller, or torque on a flap. These inputs result in the loading of powertrain components, represented by the vector  $\boldsymbol{\nu}$ , which in turn determine the dynamics of powertrain component states,  $\mathbf{x}^{PT}$ , and the dynamics of potential fault modes,  $\dot{\boldsymbol{\gamma}}$ .

Onboard sensors measure the current states of aircraft powertrain components,  $\mathbf{x}^{PT}$ , with some measurement error, denoted with the symbol  $\phi$ . Magnitudes of potential fault modes are represented by the fault mode vector,  $\boldsymbol{\gamma}$ , where fault modes are assumed to be measurable indicators of component degradation such as crack length, spall width, or pitting depth.

The loads exerted by the vehicle's active components at a given time index,  $k$ , are expressed as a function of control input signals, the current states of powertrain components, and the states of component fault modes that may reduce component effectiveness,

$$\boldsymbol{\nu}_k = f^{PT}(\mathbf{u}_k, \mathbf{x}_k^{PT}, \boldsymbol{\gamma}_k, \boldsymbol{\xi}_k) \quad (1)$$

where  $\boldsymbol{\xi}$  is used to represent a vector of unknown or uncertain model parameters.

The 'Airframe Dynamics' block shown in Figure 1(a) represents the aerodynamic interactions between the vehicle air-

frame, vehicle control surfaces, and the environment. The inputs to this block are the current states of aircraft control surfaces, represented by the vector  $\mathbf{x}^{CS}$ , and the current state of the operating environment,  $\mathbf{w}$ . Environmental states represented by  $\mathbf{w}$  may include atmospheric pressure, air temperature, wind speed, and turbulence. The current state of the airframe is represented by,  $\mathbf{x}^{AF}$ ; it includes the position, heading, linear and rotational speed, and linear and rotational acceleration of the airframe in a set coordinate system.

Vehicle control surfaces are mechanically connected to powertrain components, so  $\mathbf{x}^{CS}$  should be a known function of  $\mathbf{x}^{PT}$ . The forces exerted on the vehicle's control surfaces due to their motion through surrounding air is represented here as a generic non-linear function of the airframe state, the states of vehicle control surfaces, and current environmental states,

$$\mathbf{N}_k = f^N(\mathbf{x}_k^{AF}, \mathbf{x}_k^{CS}, \mathbf{w}_k, \boldsymbol{\xi}_k) \quad (2)$$

The net forces on component control surfaces are given by the sum of the net loads exerted by powertrain components and aerodynamical pressures.

$$\mathbf{F}_{CS} = \mathbf{F}_{PT} + \mathbf{F}_{AC} \quad (3)$$

Powertrain state dynamics and airframe dynamics are generically expressed in terms of the loading vectors  $\boldsymbol{\nu}$  and  $\mathbf{N}$  as:

$$\dot{\mathbf{x}}_k^{PT} = f^{PT}(\mathbf{x}_k^{PT}, \boldsymbol{\nu}_k, \mathbf{N}_k, \boldsymbol{\xi}_k) \quad (4)$$

$$\mathbf{y}_k^{PT} = h^{PT}(\mathbf{x}_k^{PT}, \boldsymbol{\phi}_k) \quad (5)$$

$$\dot{\mathbf{x}}_k^{AF} = f^{AF}(\mathbf{x}_k^{AF}, \mathbf{x}_k^{CS}, \mathbf{w}_k, \boldsymbol{\xi}_k) \quad (6)$$

$$\mathbf{y}_k^{AF} = h^{AF}(\mathbf{x}_k^{AF}, \boldsymbol{\phi}_k) \quad (7)$$

The progression of component fault modes is represented as:

$$\dot{\boldsymbol{\gamma}}_k = f^\gamma(\mathbf{x}_k^{PT}, \boldsymbol{\gamma}_k, \boldsymbol{\nu}_k, \boldsymbol{\xi}_k) \quad (8)$$

where component failure is considered to occur when fault magnitudes exceed a defined threshold that renders the component ineffective. The deterioration of control surfaces and electromechanical components on aircraft powertrains as a function mechanical loading forces has been a topic of study for some time; examples include: electromechanical actuators (Balaban et al., 2010) and composite wing structures (Gobbato et al., 2012), to name a few. The degradation and failure of electrical components as a function of electrical power loading has also been examined for aircraft batteries (Saha et al., 2009), power electronics (Celaya et al., 2011), and electromechanical components (Byington et al., 2004).

Adequate control of aircraft does not in most cases require a pilot to understand environmental dynamics or the internal dynamics of the flight vehicle in great detail. In this paper, pilots or autopilots are considered to make decisions based on an internal decision making policy that maps observations

of  $\mathbf{y}_k^{AF}$  and  $\mathbf{y}_k^{PT}$  at time-index  $k$  to appropriate control outputs,  $\mathbf{u}_k$ . An autopilot will use an embedded control policy to map  $(\mathbf{y}_k^{AF}, \mathbf{y}_k^{PT}) \rightarrow \mathbf{u}_k$ . For human pilots the mapping  $(\mathbf{y}_k^{AF}, \mathbf{y}_k^{PT}) \rightarrow \mathbf{u}_k$  will be determined by the pilot's situational awareness and judgment. The mechanism for interaction between an autopilot and supervisory failure prognostics and decision making routines may be for the decision making routines to directly update the autopilot's control policy. Policy updates for human pilots could be prompted indirectly by presenting the pilot with system health information and suggested risk mitigating actions as described in (Bukov et al., 2007).

Figure 1(b) shows a block diagram of the framework for simulating inner-loop vehicle dynamics. The framework includes a pilot that will provide closed-loop control of a simulated aircraft. Aircraft vehicle dynamics are simulated in the proposed framework using the commercially available software X-Plane<sup>1</sup>.

Sensor measurements of vehicle states are simulated using simulated sensors and simulated noise. Additional software modeling or hardware components may be plugged into the SIL/HIL testing framework to provide offline simulations of the powertrain energy conversion dynamics monitored by outer-loop supervisory control routines. The functionality exists within X-Plane to model electric power trains; however, that capacity was not explored for this paper.

Communication between an autopilot board and the framework is facilitated by the open-source program APM Mission Planner<sup>2</sup>. The X-Plane Toolbox for MATLAB was used to communicate with APM Mission Planner, X-Plane, and outer-loop supervisory control routines running in Matlab. The toolbox, currently being developed at NASA Ames Research Center, provides various Matlab functions that allow for UDP communication with an associated X-Plane plug-in and APM Mission Planner. The team developing the toolbox intends to release it open-source upon completion.

A hardware-only recreation of the 'Flight Control Mechanisms' portion of the inner-loop vehicle dynamics, illustrated in Figure 1(b), could be accomplished in a laboratory setting using an aircraft battery pack, power electronic motor/actuator drivers, electromechanical components, and associated interconnection cabling. Pilot controls could be sent directly to an electrical power distribution system assembled in the laboratory, and additional loading hardware could be used to apply mechanical loads to the electromechanical components of the powertrain in order to recreate the environmental loads estimated by the aircraft simulator. This approach is similar in nature to dynamometer testing commonly performed in the testing of automotive systems (Kelly et al., 2002; Tsang et al., 1985). Software models may be switched

<sup>1</sup>[www.x-plane.com/](http://www.x-plane.com/)

<sup>2</sup><http://code.google.com/p/ardupilot-mega/wiki/Mission>

in for some or all of the hardware components in this setup; however, small errors in modeling the behavior of a given component may have outsized effects in observed system behavior over long time periods.

## 2.2. Outer-loop Failure Prognostics and Decision Making

Supervisory outer-loop control routines use sensor measurements to estimate current and future system states given approximations of system state dynamics and physics of failure models. The Bayesian belief in the system state at time-index  $k$ , given of sequential observations from time-index 0 to  $k$ , is:

$$p(\mathbf{x}_k | \mathbf{y}_k) = \alpha p(\mathbf{y}_k | \mathbf{x}_k) \cdot \int p(\mathbf{x}_k | \mathbf{x}_{k-1}, \mathbf{u}_{k-1}) \cdot p(\mathbf{x}_{k-1} | \mathbf{y}_{k-1}) d\mathbf{x}_{k-1} \quad (9)$$

where  $\mathbf{x}_k$  and  $\mathbf{y}_k$  represent the system state and measured sensor output information respectively,  $p(\mathbf{y}_k | \mathbf{x}_k)$  represents the probability distribution for measured outputs given a known system state,  $p(\mathbf{x}_k | \mathbf{x}_{k-1}, \mathbf{u}_{k-1})$  represents an uncertain model for system state dynamics, and  $\alpha$  is a normalizing constant.

As described in Section 2.1, the input-output response of the system is expected to be dependent on the states several unknown model parameters and the states of potential component fault modes. A Bayesian belief expression similar to the one given in Eq. (9) could also be used to express belief in the current states of fault magnitudes or other model parameters based on a history of observations of the system's input-output dynamics, as discussed in the following references (Baram & Sandell, 1978; Collins et al., 1974; Saha & Goebel, 2008).

Probability distributions for belief in the current states of  $\mathbf{x}_k^{PT}$ ,  $\mathbf{x}_k^{AF}$ , and  $\gamma_k$ , based on a history of observations of  $\mathbf{y}_{0:k}^{PT}$ ,  $\mathbf{y}_{0:k}^{AF}$ , and  $\mathbf{u}_{0:k}^{AF}$  are generically represented in Figure 2.1 as:

$$p(\mathbf{x}_k^{PT}, \mathbf{x}_k^{AF}, \gamma_k | \mathbf{y}_{0:k}^{PT}, \mathbf{y}_{0:k}^{AF}, \mathbf{u}_{0:k}) \quad (10)$$

Many Bayesian and machine learning methods have been published for the estimation of such probability distributions in the aviation domain (Lopez & Sarigul-Klijn, 2010; Napolitano et al., 1998).

Prediction of the evolution of future system states may be performed by propagating input uncertainty, model uncertainty, and state uncertainty forward in time. In the case of component remaining useful life (RUL) prediction during an aircraft flight, predictions of the evolution of component loads and corresponding predictions of fault state evolution are extended into the future until there is sufficient confidence in the occurrence of either component failure or completion of a prescribed flight plan. Particle filtering (Arulampalam, Maskell, Gordon, & Clapp, 2002), extended Kalman filtering (Ray & Tangirala, 4), and Markov modeling (Guidaa &



Figure 2. Edge-540 on runway

Pulcini, 2011) are examples of predictive filtering techniques used to propagate current state and model uncertainties forward in time.

The role of stochastic estimates of future loading in prognostic predictions is described in (Sankararaman et al., 2013; Tang et al., 2009). Because inner-loop control policies may be modified by outer-loop supervisory control actions, the outer-loop prognostics and decision making routines could also be factored into the computation of future component load estimates. (Bole et al., 2012) describes the incorporation of outer-loop control policies into inner-loop fault growth predictions. In offline simulations stochastic beliefs about the manner in which the environment or system will evolve over time may be validated against repeated randomized simulations of flight scenarios.

## 3. A CASE STUDY: UAV BATTERY CHARGE DEPLETION MODELING

This section illustrates the implementation of the proposed SIL/HIL framework for the offline simulation of battery charge depletion onboard a prototype electric UAV platform. The framework is intended to be used here for the offline V&V testing of battery charged depletion prediction and decision making routines. The aircraft platform for this case study is a commercial-off-the-shelf (COTS) 33% scale model of the Zivko Edge 540T airplane, pictured in Figure 2. The electrical and mechanical connections in the UAV powertrain are illustrated in Figure 3. The propeller of the UAV is driven by two tandem mounted out runner brushless DC motors that are each powered by a series connection of two lithium polymer battery packs. Each of the battery packs consist of five series connections of two 4.2V 3900mAh lithium polymer pouch cells wired in parallel. Power flow from the battery packs to the driving motors is controlled by a Jeti 90 Pro Opto electric speed controller (ESC) board. The ESC board sends synchronized voltages to the propeller motors at a duty cycle determined by a throttle input. The throttle input is either sent by remote control from a pilot, or by an onboard autopilot.

The Edge 540 research vehicle is operated either remotely by a pilot on the ground, or by an onboard autopilot routine.

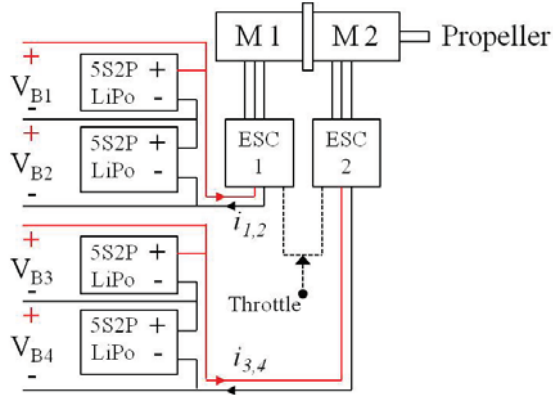


Figure 3. Electrical and mechanical connections of an Edge-540 UAV powertrain

During both remote control and autonomous flight a human pilot will maintain line of sight with the aircraft, and stand ready to execute a landing maneuver when the command is given by other operators on the ground that are monitoring the battery end-of-discharge prognostics and decision making data from the aircraft.

Charge estimation and end of charge prediction for UAV powertrain batteries has previously been examined in several publications by Bhaskar Saha at NASA ARC, Quach Chong Chi at NASA LaRC, and others (Saha, Quach, & Goebel, 2011; Saha, Koshimoto, et al., 2011). A separate battery system is used to power the data acquisition and other flight communications and control hardware. The two battery systems are sized such that it is very likely that the batteries powering the propeller motors will be the first to be depleted. For that reason, onboard battery discharge prognostic algorithms and supervisory decision making actions are considered to only be concerned with the propeller driving batteries.

Implementation of the SIL/HIL framework is described in three parts: inner-loop controls, power battery modeling, and battery demand modeling.

### 3.1. The Inner-Loop Controller

Inner-loop controls are considered to be generated from pilot or autopilot that regulates aircraft throttle and actuator controls according to an internal control policy, just as it would onboard the aircraft. Vehicle flight plans are considered to be given in terms of an ordered set of 3D coordinates to be visited by the UAV, and a desired airspeed for making the translation from one waypoint to the next.

Autonomous control of the Edge 540 is performed using an ArduPilot board. The ArduPilot works to follow a specified flight plan based on a set of PID control parameters, tuned prior to flight, and periodic measurements of vehicle airspeed, heading, and GPS position. As shown in Figure 1(b), the closed-loop performance of inner-loop aircraft con-

trol routines may be simulated over a variety of flight plans and environmental conditions using the X-Plane flight simulator. Plane Maker, A design tool within the X-Plane package, was used to specify the aircraft mass, balance, and geometry for use in X-Plane aerodynamic simulations. APM mission planner, an open source software package is used to communicate with the ArduPilot board, and to translate the simulated aircraft state data generated by X-Plane into the sensor signals expected by the ArduPilot. There is some unavoidable error between the actual geometry, drag, and mass distribution of the aircraft and that used in the X-Plane aerodynamics models; however, because the control system is closed-loop small errors in simulating aircraft aerodynamics will not typically accumulate into large errors.

This configuration allows for the thorough testing of algorithm performance and safety before conducting flight tests. X-Plane can simulate various weather conditions and hardware configurations, and the ArduPilot can be tested with various flight plans.

### 3.2. The Battery Model

The outer-loop routines are considered to be focused on the depletion of battery charge. Onboard outer-loop routines will estimate the charge remaining in the aircraft's batteries using domain knowledge and periodic measurements of battery current and voltage (Pang, Farrell, Du, & Barth, 2001).

Battery voltage-current dynamics may be recreated over simulated flights in a laboratory by loading real or simulated batteries with a current indicative of flight loads. It should be noted however that battery dynamics will vary substantially as a function battery health and temperature (Jossen, 2006). Differences in state of health and thermal loading of real and simulated batteries may cause results from SIL/HIL cycling of batteries in a laboratory to diverge from the observed battery dynamics in flight test.

Aircraft powertrain batteries are simulated in SIL testing using the equivalent circuit model shown in Figure 4. This battery model uses six electrical components that are tuned to recreate the observed current-voltage dynamics of Edge 540 powertrain batteries. Battery charge is stored in the capacitor,  $C_b$ . The  $R_s, C_s$  and  $R_{cp}, C_{cp}$  pairs capture internal resistance drops and concentration polarization effects, respectively. The resistor  $R_p$  accounts for battery self-discharge over time.

Because battery current-voltage dynamics are known to vary as a function of battery SOC some of the resistive and capacitive (RC) components in the equivalent circuit model must be parameterized as functions of battery SOC (Zhang & Chow, 2010). It was decided based on qualitative observation that defining  $C_b, C_{cp}$ , and  $R_{cp}$  as parameterized functions of battery SOC gave an acceptable trade-off between the number of

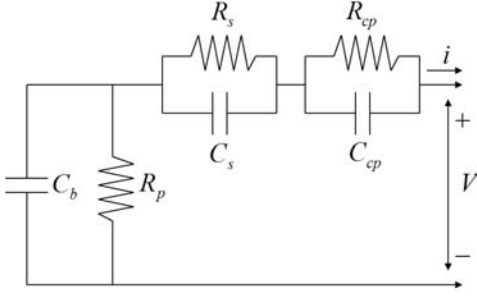


Figure 4. Equivalent circuit battery model

Parameter	Value	Parameter	Value
$q_{max}$	$2.88 \times 10^4$ C	$C_s$	89.3 F
$C_{max}$	$2.85 \times 10^4$ C	$R_{cp0}$	$1.60 \times 10^{-3}$ $\Omega$
$C_{Cb0}$	19.4 F	$R_{cp1}$	8.45
$C_{Cb1}$	1576 F	$R_{cp2}$	-61.9
$C_{Cb2}$	41.7 F	$C_{cp0}$	2689 F
$C_{Cb3}$	-203 F	$C_{cp1}$	-2285 F
$R_s$	$2.77 \times 10^{-2}$	$C_{cp2}$	-0.73 F

Table 1. Parameter values used in equivalent circuit model

parameters to be identified and model error.

Battery SOC is defined as:

$$\text{SOC} = 1 - \frac{q_{max} - q_b}{C_{max}} \quad (11)$$

where  $q_b$  is the charge stored in the battery,  $q_{max}$  is the maximum charge of the battery, and  $C_{max}$  is the maximum charge that can be drawn from the battery. The term coulombic efficiency is used to refer to the portion of stored charge that can no longer be withdrawn after each charge-discharge cycle of the battery. Resting the battery can temporarily unlock some of its lost capacity, however the overall trend is inevitably downward.

$C_b$ ,  $C_{cp}$  and  $R_{cp}$  are parameterized as:

$$C_b = C_{Cb0} + C_{Cb1} \cdot \text{SOC} + C_{Cb2} \cdot \text{SOC}^2 + C_{Cb3} \cdot \text{SOC}^3 \quad (12)$$

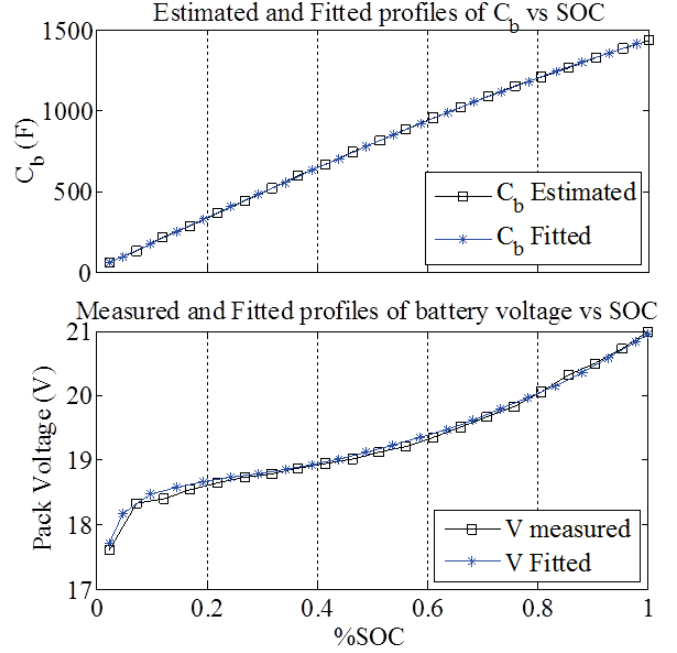
$$C_{cp} = C_{cp0} + C_{cp1} \cdot \exp(C_{cp2} (1 - \text{SOC})) \quad (13)$$

$$R_{cp} = R_{cp0} + R_{cp1} \cdot \exp(R_{cp2} (1 - \text{SOC})) \quad (14)$$

where the parameterization coefficients are tuned based on observed current-voltage battery data over a SOC range. Values for all of the RC components and parameterization coefficients used are defined in Table 1.

The current and voltage dynamics of the equivalent circuit model are defined as:

$$x^B = [q_b \quad q_{cp} \quad q_{Cs}]^T \quad (15)$$

Figure 5. Measured and fitted profiles for  $C_b$  and battery voltage

$$\dot{x}^B = \begin{bmatrix} -\frac{1}{C_b R_p} & \frac{1}{C_{cp} R_p} & \frac{1}{C_s R_p} \\ \frac{1}{C_b R_p} & -\frac{1}{C_{cp} R_p R_{cp}} & \frac{1}{C_s R_p} \\ \frac{1}{C_b R_p} & \frac{1}{C_{cp} R_p} & \frac{1}{C_s R_p} \end{bmatrix} x + \begin{bmatrix} i \\ i \\ i \end{bmatrix} + \xi \quad (16)$$

$$y^B = V_p = \begin{bmatrix} \frac{1}{C_b} & \frac{1}{C_{cp}} & \frac{1}{C_s} \end{bmatrix} \cdot x \quad (17)$$

where  $q_b$ ,  $q_{cp}$ , and  $q_{Cs}$  represent the charge stored in  $C_b$ ,  $C_{cp}$ , and  $C_{Cs}$  respectively. The total voltage drop across the battery terminals,  $V_p$ , is given by the sum of the voltage drops across the each of the three capacitors in the equivalent circuit model.

The RC parameters in the equivalent circuit model are identified using data from two battery characterization experiments. The first experiment is a low current discharge of a battery from a fully charged state until a cutoff voltage of 17.5V is reached. This type of discharge is mostly affected by the  $C_b$ ,  $q_b$ ,  $q_{max}$ , and  $C_{max}$  parameters in the model. Figure 5 shows a polynomial fit of  $C_b$  as a function of SOC, and the battery voltage fit for the tuned parameter values for  $C_{Cb0}$ ,  $C_{Cb1}$ ,  $C_{Cb2}$ ,  $C_{Cb3}$ ,  $q_{max}$ , and  $C_{max}$ .

A pulsed loading experiment is used to fit the remaining parameters in the equivalent circuit model to the observed changes in battery hysteresis behavior as a function of SOC. Figure 6 shows the battery voltage fit over a pulsed loading profile.

Observed battery loading over a piloted flight of the Edge 540 is shown in Figure 7. As was shown in Figure 3, batteries B2 and B4 are wired in series with batteries B1 and B3 respec-

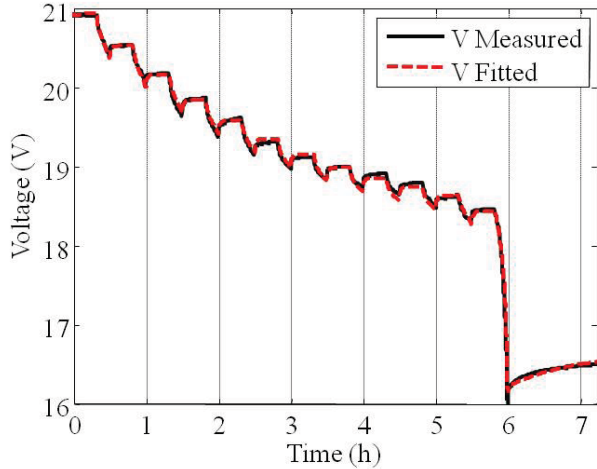


Figure 6. Measured and fitted profiles for battery voltage during pulsed loading

tively, so the current flowing through series connected batteries is equal. An asymmetric loading of the two propeller motors over the sample flight is apparent from the battery loads given in Figure 7. Motor M2 is known to consistently draw more current than motor M1 on the Edge 540, due to unregulated coupling of the two motor electron speed controls (ESCs). Predicted and measured voltage profiles for batteries B1 and B3 using the recorded battery current profiles are shown in Figure 7. The close match between observed battery voltages and open-loop predictions over a given loading profile provides a measure of the validity of the software model.

The tuned battery model may be used to estimate the internal SOC of powertrain batteries based on sampled voltage and current data. The output of model based filtering approaches such as Kalman filtering will be much less susceptible to initialization and measurement errors than the Coulomb counting method currently used in many battery monitoring systems (Dai, Wei, & Sun, 2006).

### 3.3. Battery Demand Modeling

The proposed SIL/HIL testbed separates the simulation of aerodynamics and powertrain dynamics into two functional blocks. Connecting these two blocks requires that the airframe loads reported by the aerodynamics simulation be translated into loads on the system's powertrain components. In practice, the lack of direct measurements for airframe loads such as component forces and torques increases the difficulty of this mapping.

Tuning and validation of a propeller load mapping function is separated into two steps in this paper. First, a series of characterization experiments are performed in X-Plane to identify a nonlinear mapping between propeller output power and aircraft angle of climb, speed, and acceleration. Second, the

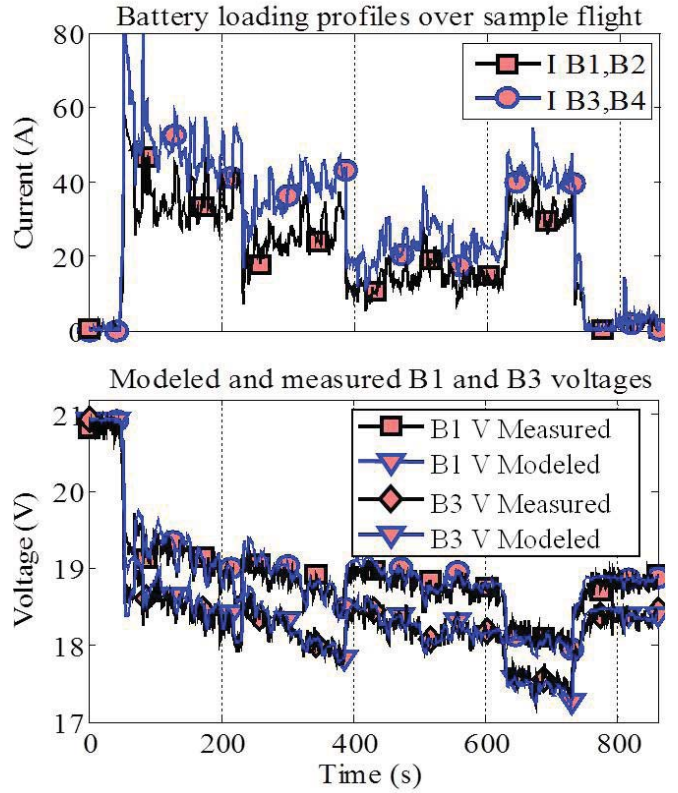


Figure 7. Modeled and measured voltages of batteries B1 and B3 for a sample flight loading profile

modeled propeller power is mapped to a required battery power using a fixed power conversion efficiency coefficient and a proportional drag correction coefficient.

The nonlinear relationship between propeller output power and aircraft angle of climb, speed, and acceleration is observed in X-Plane simulations by performing a series of climbing and descending maneuvers at various angle of climb and throttle setpoints. This experiment is used to fit a general set of aircraft aerodynamics and energy conservation equations. The equations below are developed using the following assumptions: 1) the propeller is mounted on the aircraft nose; 2) the angle between the thrust vector generated by the propeller and the velocity vector of the aircraft is small; 3) Turning forces are small in comparison to thrust and drag forces in the direction of travel.

The sum of the forces acting in the aircraft direction of travel is given by

$$T_{x_w} = D(v) + m \cdot g \cdot \sin(\gamma) + m \cdot \dot{v} \quad (18)$$

where  $T_{x_w}$  is the net force on the aircraft in the direction of travel,  $D$  is the drag force acting in the opposite direction of aircraft motion,  $v$  is the aircraft speed,  $\dot{v}$  is acceleration,  $\gamma$  is angle of climb,  $m$  is the vehicle mass, and  $g$  is total accelera-

tion due to gravity.

The mass of the instrumented Edge 540 is approximately 44lbs. The drag force on the airframe is represented by the following polynomial function of airspeed and angle of climb.

$$D(v, \gamma) = c_1 + c_2 \cdot v + c_3 \cdot v^2 + c_4 \cdot \gamma \quad (19)$$

Figure 8(a) shows a fit of the drag model to the averaged drag force reported by the X-Plane simulator over several steady speed climbing and descending maneuvers. The fitted parameter values are:  $c_1 = 13.47$ ,  $c_2 = -0.6$ ,  $c_3 = 0.019$ ,  $c_4 = 0.14$ . During take-off and landing maneuvers when the aircraft speed is less than the stall speed of the aircraft the drag force is approximated as  $D = 3 \cdot$

A plot of the measured and estimated propeller thrust versus airspeed is shown in Figure 8(b). The model fit is shown to be very close except at speeds near the stall speed of the aircraft, which is approximately  $15m/s$ .

The product of thrust and airspeed gives the motive power exerted by the aircraft. A proportional relationship is used to model the ratio between the power output of the propeller and the resulting motive power:

$$P_p = \frac{1}{\eta_p} \cdot T_{x_w} \cdot v \quad (20)$$

where  $P_p$  represents propeller output power, which is the product of its torque and speed, and  $\eta_p$  represents the approximate propeller output power conversion efficiency. Figure 10 shows the modeled propeller power and that reported by the X-Plane simulator for several steady speed climbing and descending maneuvers. The  $\eta_p$  parameter for the modeled aircraft is fit to  $\eta_p = 0.7652$ .

Conversion between the propeller power to maintain an airspeed and angle of climb is performed by assuming a fixed battery power conversion efficiency for the motors and power electronics. The combined efficiency of the aircraft motors and onboard power electronics is expressed as the ratio of battery power input to motor power output,

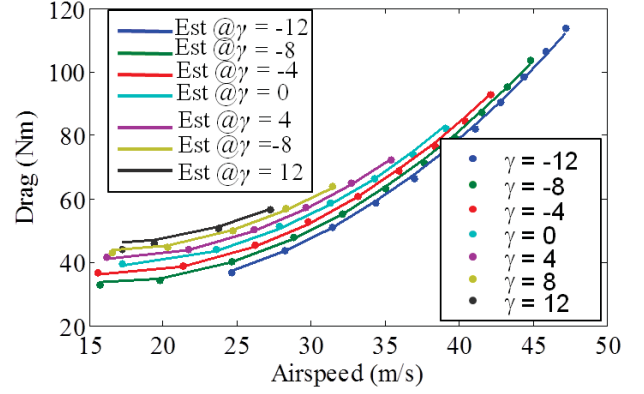
$$P_p = \frac{1}{\eta_e} \cdot P_b \quad (21)$$

where  $\eta_e$  represents power conversion efficiency.

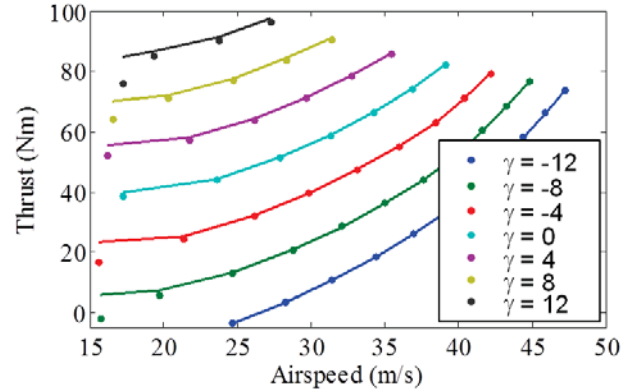
A proportional drag correction coefficient is introduced to scale the drag model fit using the X-Plane generated data by a fixed ratio to match observed aircraft dynamics,

$$D_A(v, \gamma) = \lambda_D \cdot D_M(v, \gamma) \quad (22)$$

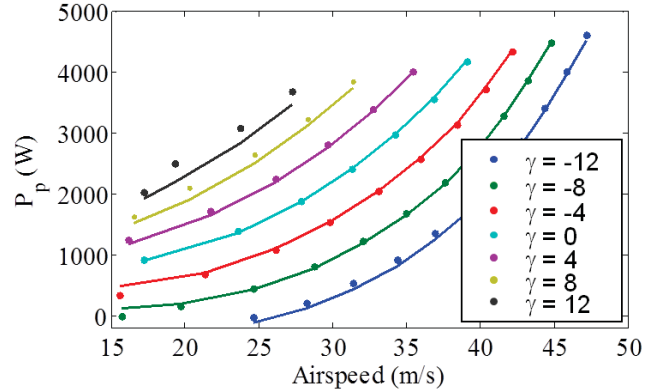
where  $D_A$  and  $D_M$  represent the drag forces seen by the actual aircraft and the fitted model respectively at a given vehicle speed and angle of climb, and  $\lambda_D$  is an approximated constant of proportionality.  $\eta_e = 0.85$  and  $\lambda_D = 0.9$  were



(a) Estimated and measured drag vs airspeed at various angles of climb



(b) Estimated and measured thrust vs airspeed at various angles of climb



(c) Estimated and measured propeller power output vs airspeed at various angles of climb

Figure 8. Model fitting results for X-Plane flight load characterization tests

fitted using flight data.

A roughly proportional deviation between the modeled and actual drag force is attributed to slight errors in modeling the aircraft geometry and surface aberrations. Small errors in modeling aircraft drag will cause only small effects on the aircraft handling from the perspective of a pilot or an autopi-

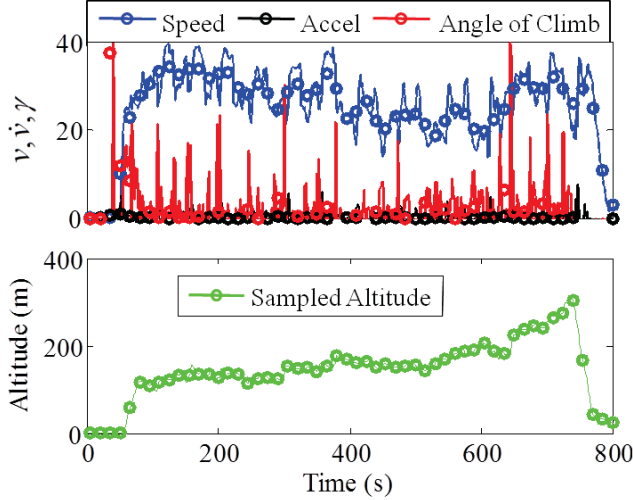


Figure 9. Approximate aircraft airspeed, acceleration, and angle of climb measurements derived from GPS samples

lot, so the drag correction need not necessarily be made for the SIL testing of that control loop. However, small errors in approximating loads on onboard energy storage devices will accumulate into large errors over a simulated flight.

Substitution of Eqns. (21) and (22) into Eqns. (18)-(20) yield the approximate battery power required to fly at a particular airspeed and angle of climb.

$$P_B = \frac{1}{\eta_e \eta_p} \cdot T_{x_w} \cdot v$$

$$P_B = \frac{v}{\eta_e \eta_p} \cdot (D_A(v, \gamma) + mg \cdot \sin(\gamma) + m\dot{v}) \quad (23)$$

$$P_B = \frac{v}{\eta_e \eta_p} \cdot (\lambda_D D_M(v, \gamma) + mg \cdot \sin(\gamma) + m\dot{v})$$

Figure 9 shows approximate aircraft airspeed, acceleration, and angle of climb measurements derived from GPS samples over a sample aircraft flight. Measurements were taken at fifteen second intervals. Figure 10 shows the predicted and measured battery power draw over the sample aircraft flight. The battery power predictions shown in Figure 10 are made using periodic samples of airspeed, acceleration, and angle of climb. The battery power predictions shown in Figure 10 are seen to match the observed power draw fairly well over the sample flight, aside from an apparent under prediction of battery power required during takeoff. The under prediction of power required during takeoff could arise in part from the assumption that the angle between the thrust vector and the velocity vector is small, which is not necessarily the case during takeoff. The battery power demand modeling used here also does not account for the fact that motor power conversion efficiency is typically very low during initial spin up.

Battery output power is equal to the product of current and voltage. Given an estimate of the battery power output required to fly a particular maneuver, and knowledge of the division of power between the two propeller motors, the current

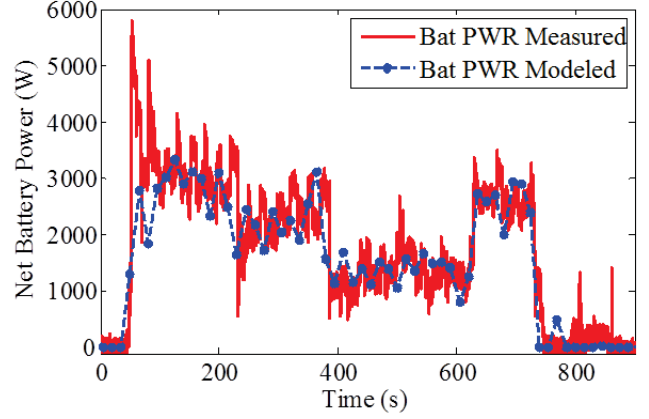


Figure 10. Measured and modeled battery power output

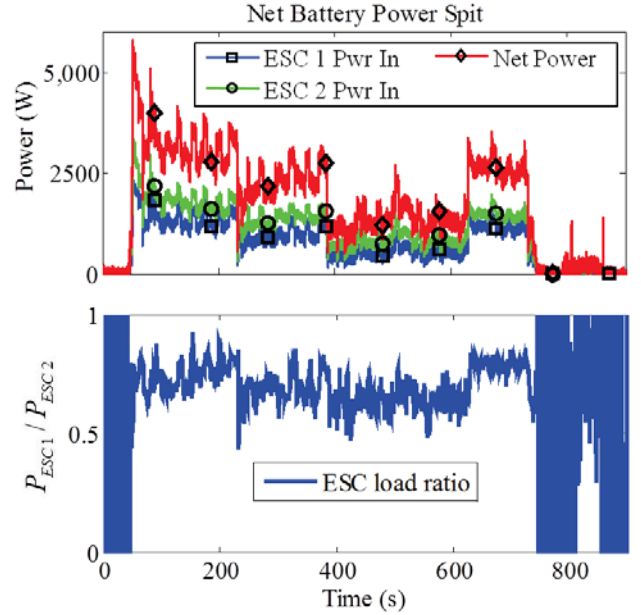


Figure 11. Measured battery power input to ESCs (Top) and observed ESC power ratio over a sample flight (bottom)

loads on each of the series connected battery packs is given by:

$$I_{1,2} = \frac{\lambda_{ESC} P_b}{(\lambda_{ESC} + 1) \cdot (V_{B1} + V_{B2})} \quad (24)$$

$$I_{3,4} = \frac{P_b}{(\lambda_{ESC} + 1) \cdot (V_{B3} + V_{B4})}$$

where  $\lambda_{ESC}$  represents the ratio of battery power drawn by each of the onboard ESCs.

$$\lambda_{ESC} = \frac{I_{1,2} \cdot (V_{B1} + V_{B2})}{I_{3,4} \cdot (V_{B3} + V_{B4})} \quad (25)$$

Figure 11 shows the observed ratio of battery power drawn from each of the onboard ESCs over a sample flight. The ratio of ESC power draw is currently uncontrolled, and it is seen to drift around a value of  $\lambda_{ESC} \approx 0.7$  over the sample flight.

The approximation for  $\lambda_{ESC}$  to be used in SIL and HIL testing of the vehicle powertrain may be improved in future work by incorporating possible dependencies on time, battery pack voltage, throttle command, and other inputs control inputs.

#### 4. CONCLUSIONS

A framework is described for the offline recreation of dynamic loads on simulated or physical aircraft powertrain components based on a real-time simulation of airframe dynamics running in the X-Plane flight simulation software package, an inner-loop flight control policy executed by either an autopilot routine or a human pilot, and a supervisory outer-loop control policy. The creation of an offline framework for verifying and validating supervisory outer-loop prognostics and decision making routines is described for the example of battery charge depletion failure scenarios onboard a prototype Edge 540 UAV with electric propulsion. The SIL/HIL testbed described in this paper is intended to be used to perform much more comprehensive and cost-effective testing of aircraft fault prognostics and decision making tools than would be practical to conduct in flight testing.

#### ACKNOWLEDGMENT

PCoE, etc.

#### NOMENCLATURE

$x^{AF}$	airframe state vector
$y^{AF}$	observation of airframe state vector
$x^{PT}$	electrical power dist. system state vector
$y^{PT}$	observation of $x^{PT}$ states
$u$	pilot or autopilot control output vector
$\nu$	mechanical loads on electromechanical components
$\nu$	net mechanical loads exerted by airframe
$w$	environmental state parameter vector
$\gamma$	magnitude state vector for potential faults modes
$\xi$	captures uncertainties in physics of failure models
$\phi$	captures uncertainties in physics of failure models

#### REFERENCES

- Arulampalam, M. S., Maskell, S., Gordon, N., & Clapp, T. (2002). A tutorial on particle filters for online nonlinear/non-gaussian bayesian tracking. *IEEE Transactions on Signal Processing*, 50(2), 174-188.
- Balaban, E., Saxena, A., Narasimhan, S., Roychoudhury, I., Goebel, K., & Koopmans, M. (2010). Airborne electro-mechanical actuator test stand for development of prognostic health management systems. In *Annual conference of the prognostics and health management society*.
- Baram, Y., & Sandell, N. (1978). An information theoretic approach to dynamical systems modeling and identification. *IEEE Transactions on Automatic Control*, 23, 61-66.
- Bole, B., Goebel, K., & Vachtsevanos, G. (2012). Stochastic modeling of component fault growth over a derived domain of fiesible output control effort modifications. In *Annual conference of the prognostics and health management society*.
- Brown, A., & Garcia, R. (2009). Concepts and validation of a small-scale rotorcraft proportional integral derivative (pid) controller in a unique simulation environment. *Unmanned Aircraft Systems, I*, 511-532.
- Bukov, V., Chernyshov, V., Kirk, B., & Schagaev, I. (2007). Principle of active system safety for aviation: Challenges, supportive theory, implementation, application and future. In *Astec*.
- Byington, C., Watson, M., Edwards, D., & Stoelting, P. (2004). A model-based approach to prognostics and health management for flight control actuators. In *Ieee aerospace conference*.
- Celaya, J., Kulkarni, C., Biswas, G., & Goebel, K. (2011). A model-based prognostics methodology for electrolytic capacitors based on electrical overstress accelerated aging. In *Proceedings of the annual conference of the phm society*.
- Collins, J., Har, G., Haselman, T. K., & Kennedy, B. (1974). Statistical identification of structures. *AIAA journal*, 12, 185-190.
- Dai, H., Wei, X., & Sun, Z. (2006). Online soc estimation of high-power lithium-ion batteries used on hevs. In *Ieee international conference on vehicular electronics and safety*.
- Gobbato, M., Conte, J., Kosmatka, J., & Farrar, C. (2012). A reliability-based framework for fatigue damage prognosis of composite aircraft structures. *Probabilistic Engineering Mechanics*, 29, 176-188.
- Guidaa, M., & Pulcini, G. (2011). A continuous-state Markov model for age- and state-dependent degradation processes. *Structural Safety*, 33(6), 354-366.
- ibeiro, L., & Oliveira, N. M. (2010). Uav autopilot controllers test platform using matlab/simulink and x-plane. In *Frontiers in education conference (fie)*.
- Jossen, A. (2006). Fundamentals of battery dynamics. *Journal of power sources*, 154, 530-538.
- Kelly, K., Mihalic, M., & Zolot, M. (2002). Battery usage and thermal performance of the toyota prius and honda insight during chassis dynamometer testing. In *Seventeenth annual ieee battery conference on applications and advances*.
- Lopez, I., & Sarigul-Klijn, N. (2010). A review of uncertainty in flight vehicle structural damage monitoring, diagnosis and control: Challenges and opportunities. *Progress in Aerospace Sciences*, 46, 247-273.
- Napolitano, M., Windon, D., Casanova, J., Innocenti, M., & Silvestri, G. (1998). Kalman filters and neural-network

schemes for sensor validation in flight control systems. In *IEEE transactions on control systems technology*.

- Pang, S., Farrell, J., Du, J., & Barth, M. (2001). Battery state-of-charge estimation. In *American control conference*.
- Ray, A., & Tangirala, S. (4). Stochastic modeling of fatigue crack dynamics for on-line failure prognostics. *IEEE Transactions on Control Systems Technology*, 1996, 443-451.
- Sagoo, G., Gururajan, S., Seanor, B., Napolitano, M., Perhinschi, M., Gu, Y., & Campa, G. (2010). Evaluation of a fault-tolerant scheme in a six-degree-of-freedom motion flight simulator. *Journal of Aerospace Computing, Information, and Communication*, 7, 47-67.
- Saha, B., & Goebel, K. (2008). Uncertainty management for diagnostics and prognostics of batteries using Bayesian techniques. In *Ieee aerospace conference*.
- Saha, B., Goebel, K., Poll, S., & Christophersen, J. (2009). Prognostics methods for battery health monitoring using a Bayesian framework. *IEEE Transactions on Instrumentation and Measurement*, 58(2), 291-296.
- Saha, B., Koshimoto, E., Quach, C. C., Hogge, E. F., Strom, T. H., Hil, B. L., ... Goebel, K. (2011). Battery health management system for electric UAVs. In *Ieee aerospace conference*.
- Saha, B., Quach, P., & Goebel, K. (2011). Exploring the model design space for battery health management. In *Annual conference of the prognostics and health management society*.
- Sankararaman, S., Daigle, M., Saxena, A., & Goebel, K. (2013). Analytical algorithms to quantify the uncertainty in remaining useful life prediction. In *Ieee aerospace conference*.
- Tang, L., Kacprzynski, G., Goebel, K., & Vachtsevanos, G. (2009). Methodologies for uncertainty management in prognostics. In *IEEE aerospace conference*.
- Tsang, P., Jacko, M., & Rhee, S. (1985). Comparison of chase and inertial brake dynamometer testing of automotive friction materials. *Wear*, 103, 217-232.
- Zhang, H., & Chow, M.-Y. (2010). Comprehensive dynamic battery modeling for PHEV applications. In *Ieee power and energy society general meeting*.

## BIOGRAPHIES



**Brian M. Bole** graduated from the FSU-FAMU School of Engineering in 2008 with a B.S. in Electrical and Computer Engineering and a B.S. in Applied Math. Brian received a M.S. degree in Electrical Engineering from the Georgia Institute of Technology in 2011, and he is currently pursuing a Ph.D. Brian's research interests include:

analysis of stochastic processes, risk analysis, and optimization of stochastic systems. Brian is currently investigating the use of risk management and stochastic optimization tech-

niques for optimal adaptation of active component load allocations in robotic and aviation applications. In a previous project, Brian worked with the Georgia Tech EcoCar team to develop an energy management controller for optimizing the fuel economy of a charge sustaining hybrid electric vehicle.



**Christopher Teubert** received his B.S. in Aerospace Engineering from Iowa State University in 2012. While at Iowa State University, he conducted research on asteroid deflection mission design and asteroid fragment propagation for Iowa State University's Asteroid Deflection Research Center (ADRC). Previous to his current position he

worked as a spacecraft systems engineer for a Mars sample return mission as part of the NASA Academy Program. He is currently researching systems and algorithms for diagnostics, prognostics, and system health management for Stinger Ghafarian Technologies, Inc. at NASA Ames Research Center's Prognostic Center of Excellence (PCoE). He plans to begin pursuing a M.S. in 2014.



**Quach Cuong Chi** Cuong C. Quach got his M.S. from the School of Physics and Computer Sciences at Christopher Newport University in 1997. He is a staff researcher in the Safety Critical Avionics Systems Branch at NASA Langley Research Center. His research areas include development and testing of software for airframe diagnosis and strategic flight path conflict detection.



**Sixto Vazquez** obtained his MSEE degree from Old Dominion University in 1990 and BSEE from the University of Puerto Rico in 1983. He has developed real-time 3D graphical simulations to aid in the visualization and analysis of complex sensory data. Has developed techniques to interactively process, analyze, and integrate sensory data

from multiple complex, state-of-the-art sensing technologies, i.e. FMCW Coherent Laser Radar range measuring system, Bragg grating Fiber Optic Strain Sensing system, etc., into simulation.



**Kai Goebel** received the degree of Diplom-Ingenieur from the Technische Universitt Mnchen, Germany in 1990. He received the M.S. and Ph.D. from the University of California at Berkeley in 1993 and 1996, respectively. Dr. Goebel is a senior scientist at NASA Ames Research Center where he leads the Diagnostics & Prognostics groups

in the Intelligent Systems division. In addition, he directs the Prognostics Center of Excellence and he is the Associate Principal Investigator for Prognostics of NASAs Integrated

Vehicle Health Management Program. He worked at General Electric Corporate Research Center in Niskayuna, NY from 1997 to 2006 as a senior research scientist. He has carried out applied research in the areas of artificial intelligence, soft computing, and information fusion. His research interest lies in advancing these techniques for real time monitoring, diagnostics, and prognostics. He holds eleven patents and has published more than 100 papers in the area of systems health management.



**Vachtsevanos George** is a Professor Emeritus of Electrical and Computer Engineering at the Georgia Institute of Technology. He was awarded a B.E.E. degree from the City College of New York in 1962, a M.E.E. degree from New York University in 1963 and the Ph.D. degree in Electrical Engineering

from the City University of New York in 1970. He directs the Intelligent Control Systems laboratory at Georgia Tech where faculty and students are conducting research in intelligent control, neurotechnology and cardiotechnology, fault diagnosis and prognosis of large-scale dynamical systems and control technologies for Unmanned Aerial Vehicles. His work is funded by government agencies and industry. He has published over 240 technical papers and is a senior member of IEEE. Dr. Vachtsevanos was awarded the IEEE Control Systems Magazine Outstanding Paper Award for the years 2002-2003 (with L. Wills and B. Heck). He was also awarded the 2002-2003 Georgia Tech School of Electrical and Computer Engineering Distinguished Professor Award and the 2003-2004 Georgia Institute of Technology Outstanding Interdisciplinary Activities Award.